Electronic supplementary information

Visible-light-driven and selective methane conversion to oxygenates with air on halide-perovskite-based photocatalyst under mild conditions

Guang-Xing Dong,[a] Meng-Ran Zhang,[a] Ke Su,[a] Zhao-Lei Liu,[a] Min Zhang[a,b]* and Tong-Bu Lu[a]*

[a] *MOE International Joint Laboratory of Materials Microstructure, Institute for New Energy Materials and Low Carbon Technologies, School of Materials Science and Engineering, Tianjin University of Technology, Tianjin 300384, China.*

[b] *Tianjin Key Laboratory of Organic Solar Cells and Photochemical Conversion, School of Chemistry and Chemical Engineering, Tianjin University of Technology, Tianjin 300384, China.*

**Email: zm2016@email.tjut.edu.cn, lutongbu@tjut.edu.cn*

Instrumentations. XRD patterns of the as-prepared samples were collected on a Rigaku diffractometer (SmartLab, 9 kW) by Cu Kα radiation (λ = 0.15418 nm) with a scan range of 5° − 60° and a step size of 0.01°. UV−Vis DRS spectra were recorded on Lambda 750 UV/VIS/NIR spectrophotometer (Perkin Elmer) by grinding and mixing catalyst (5 mg) and barium sulfate (300 mg) thoroughly. The steady-state photoluminescence (PL) spectra were collected using a F-7000 fluorescence spectrophotometer (Hitachi) under excitation at 400 nm. The time-resolved PL measurements were carried out with a FLS-1000 steady-state and transient-state fluorescence spectrometer (Edinburgh Instruments Ltd.). Excitation wavelength: 400 nm; detection wavelength: 520 nm. TEM and HRTEM images were recorded on Tecnai G2 Spirit Twin and Talos F200 X transmission electron microscopes (FEI), respectively. HRSEM images were recorded on Verios 460L (FEI) ultrahigh-resolution scanning electron microscope. XPS measurements were carried out by an ESCALAB250Xi X-ray photoelectron spectrometer (thermo scientific) with Al Kα as the excitation source. Survey scans were collected at 1 eV resolution, whereas 0.1 eV resolution was used for high-resolution scans. The peak energies were calibrated against the binding energy of the adventitious C 1s peak, which was set at 284.8 eV. During the in-situ irradiated X-ray photoelectron spectroscopy (ISI-XPS) measurements, a 300 W Xe lamp (CEL-HXF300, CEAULICHT) with a 400 nm filter was placed about 40 cm away from the samples to investigate the electron density changes of the as-prepared photocatalysts under light irradiation and dark, respectively. The 1H NMR spectra were collected on Bruker NMR spectrometer (AVANCE III HD 400 MHz). Mass spectra of the isotope labeling experiments were obtained by a gas chromatography-mass spectrometer (Agilent, 7890B/5977B).

Product analysis. The gas reaction products were detected quantitatively using GC-2014 Gas Chromatograph instrument equipped with TCD detector (Agilent). CH_3OH was analyzed by Thermo Fisher Trace1300 Gas Chromatograph instrument equipped with headspace injector and FID detector. HCHO was analyzed through the colorimetric method. Typically, ammonium acetate (25 g), acetic acid (1 mL) and pentane-2,4-dione (0.2 mL) were dissolved in 100 mL water to form color developing reagent solution. Then 1 mL of the reaction liquid was mixed with 1 mL reagent solution. The mixed solution was placed in water bath (50 °C)

for 20 min, followed by measuring its UV−Vis absorption spectrum to detect quantitatively the concentration of HCHO based on standard curve (Fig. S11).

Fluorescence spectra of coumarin solution with photocatalysts. Coumarin was employed as a molecular probe to further analyze the •OH production in the photocatalytic system, because coumarin can easily react with •OH radical to produce 7-OH-coumarin, which has high fluorescence with characteristic peak at 453 nm, and the signal intensity is positively correlated with the concentration of •OH radical. Typically, 10 mg of photocatalyst and 10 mg coumarin were added into the mixed solvent of acetonitrile (4 mL) and water (50 μL), and the mixture was stirred for 10 min to reach an adsorption-desorption equilibrium before light irradiation. After irradiation for 2 h, the supernatant obtained by centrifugation was employed to investigate the fluorescence spectra under the excitation wavelength at 332 nm. Light source: 300 W Xe lamp, $\lambda \geq 400$ nm, 100 mW cm^{-2}.

Electron paramagnetic resonance (EPR) measurements. EPR measurements were performed on an electron paramagnetic resonance spectrometer (Bruker, EMXplus-6/1, Germany) with 5,5-dimethyl-1-pyrroline-*N*-oxide (DMPO) as the radical trapping agent. 10 μL DMPO was injection into 1 mL reaction solution dispersed with 5 mg of photocatalysts. For •OH detection, O_2 was dissolved into the mixture solution of acetonitrile and water (*V*/*V*: 3/1). Simultaneously dissolving O_2 and CH_4 into the mixture solution of acetonitrile and water (*V*/*V*: 3/1) can detect •OH and $•CH_3$ radicals. Pure methanol dissolved with O_2 was employed to detect $•O_2^-$ radicals. The mixture solution of methanol and water solution (*V*/*V*: 20/1) without O_2 was adopted to detect $•CH_2OH$ radicals. Measuring conditions: centerfield, 3500·G; sweep width, 300 G; microwave power, 2 mW; modulation frequency, 100 kHz; modulation amplitude, 1.0 G; conversion time, 30 ms; sweep time, 90 s.

Photoelectrochemical experiments. All the electrochemical measurements were carried out in a three-electrode system. FTO (0.25 cm^2) coated with photocatalyst, Pt mesh and Ag/AgCl (in 3 M KCl) were employed as the working electrode, counter electrode and reference electrode, respectively. 0.1 M $TBAPF_6$ acetonitrile solution was adopted as electrolyte. The electrochemical impedance spectroscopy (EIS) measurements were conducted under xenon lamp irradiation (100 mW cm^{-2}), and the AC voltage amplitude of 5 mV was set with

frequency range from 1 to 10^6 Hz. The photo-response of the prepared photoelectrodes ($I-t$) was evaluated by recording the photocurrent density at a bias potential of −0.4 V (*vs*. Ag/AgCl) under the same irradiation conditions.

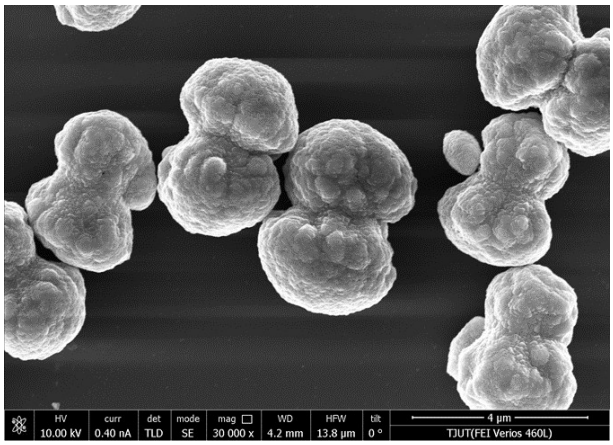

Fig. S1 SEM image of $BiVO_4$.

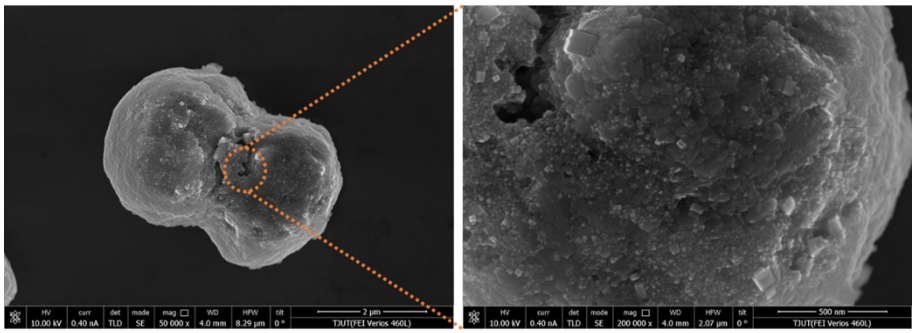

Fig. S2 SEM images of Mn@$CsPbBr_3$/$BiVO_4$.

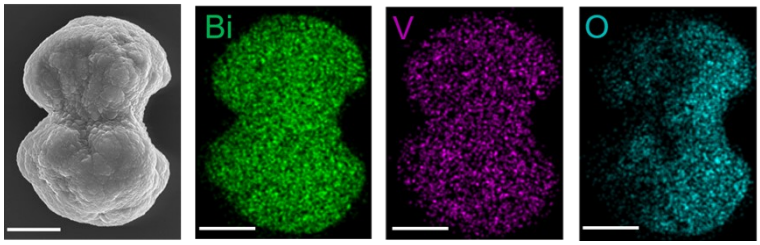

Fig. S3 SEM and elemental mapping images of $BiVO_4$ with scale bar of 1 μm.

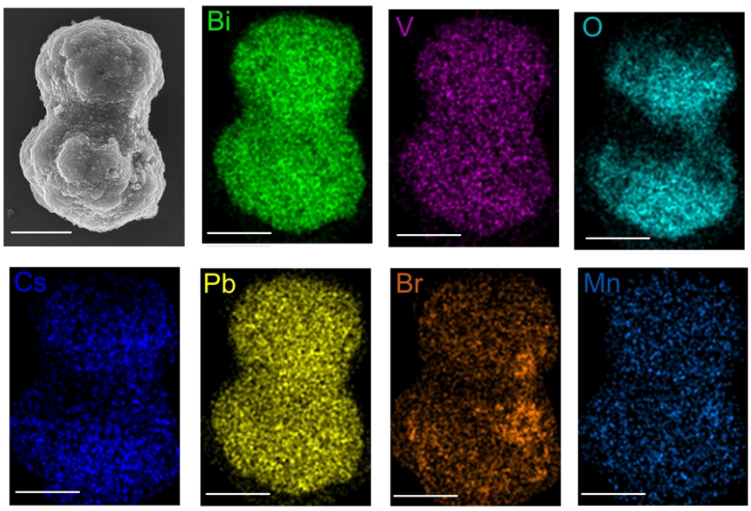

Fig. S4 SEM and elemental mapping images of Mn@$BiVO_4$/$CsPbBr_3$ with scale bar of 1 μm.

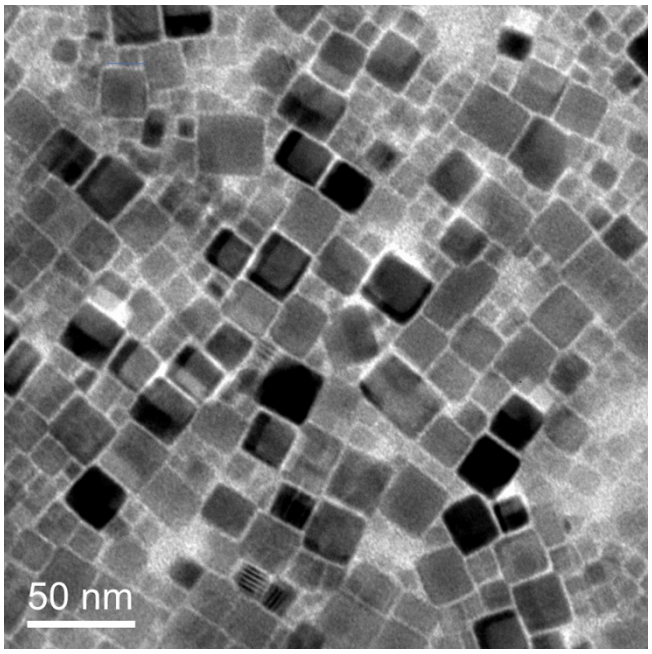

Fig. S5 TEM image of $CsPbBr_3$.

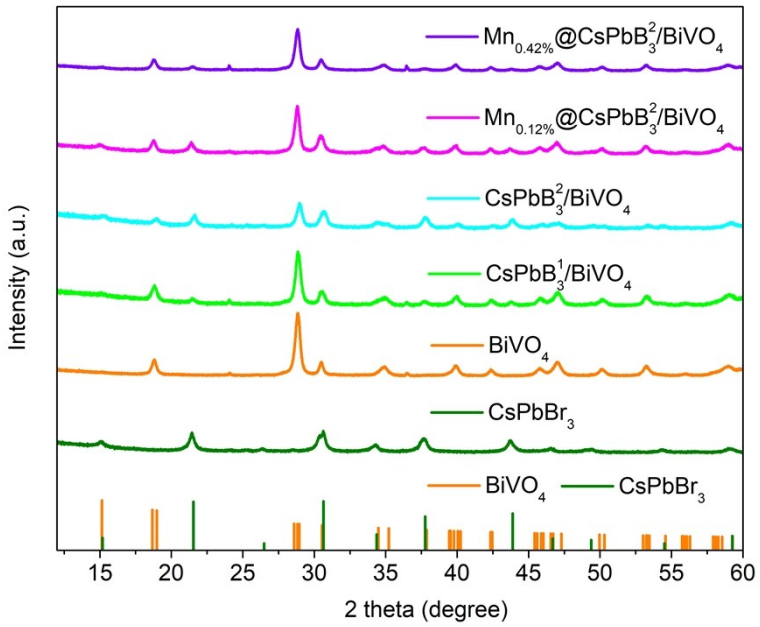

Fig. S6 XRD patterns of various photocatalysts.

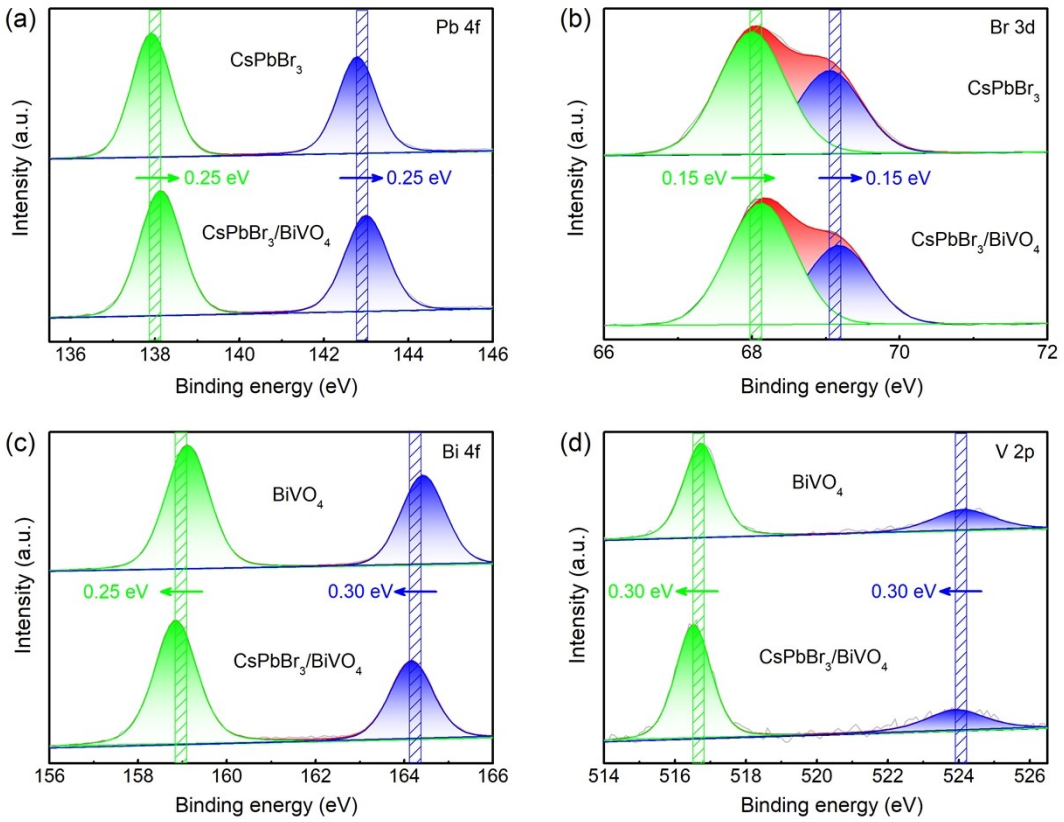

Fig. S7 High-resolution XPS spectra of $CsPbBr_3$, $BiVO_4$ and $CsPbBr_3/BiVO_4$: (a) Pb 4f, (b) Br 3d, (c) Bi 4f, and (d) V 2p.

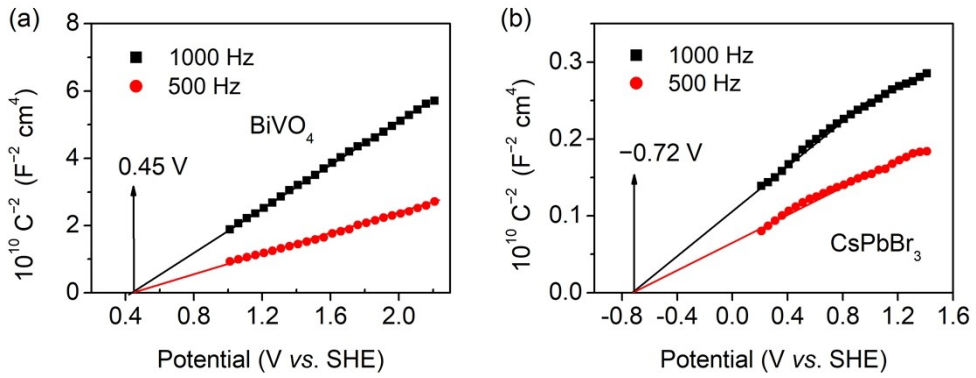

Fig. S8 Mott-Schottky plots of (a) $BiVO_4$ and (b) $CsPbBr_3$ with frequencies of 500 and 1000 Hz.

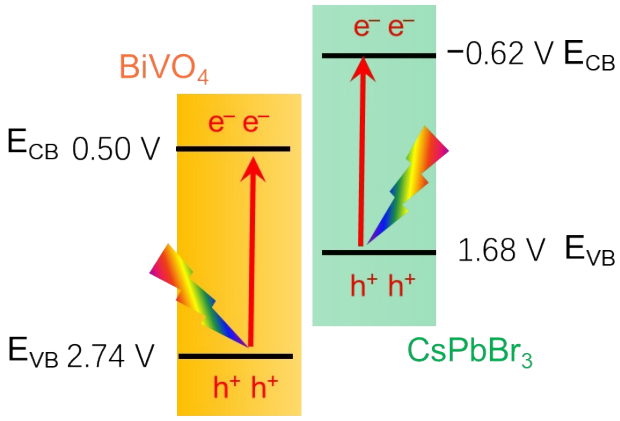

Fig. S9 Energy band structures of $CsPbBr_3$ and $BiVO_4$.

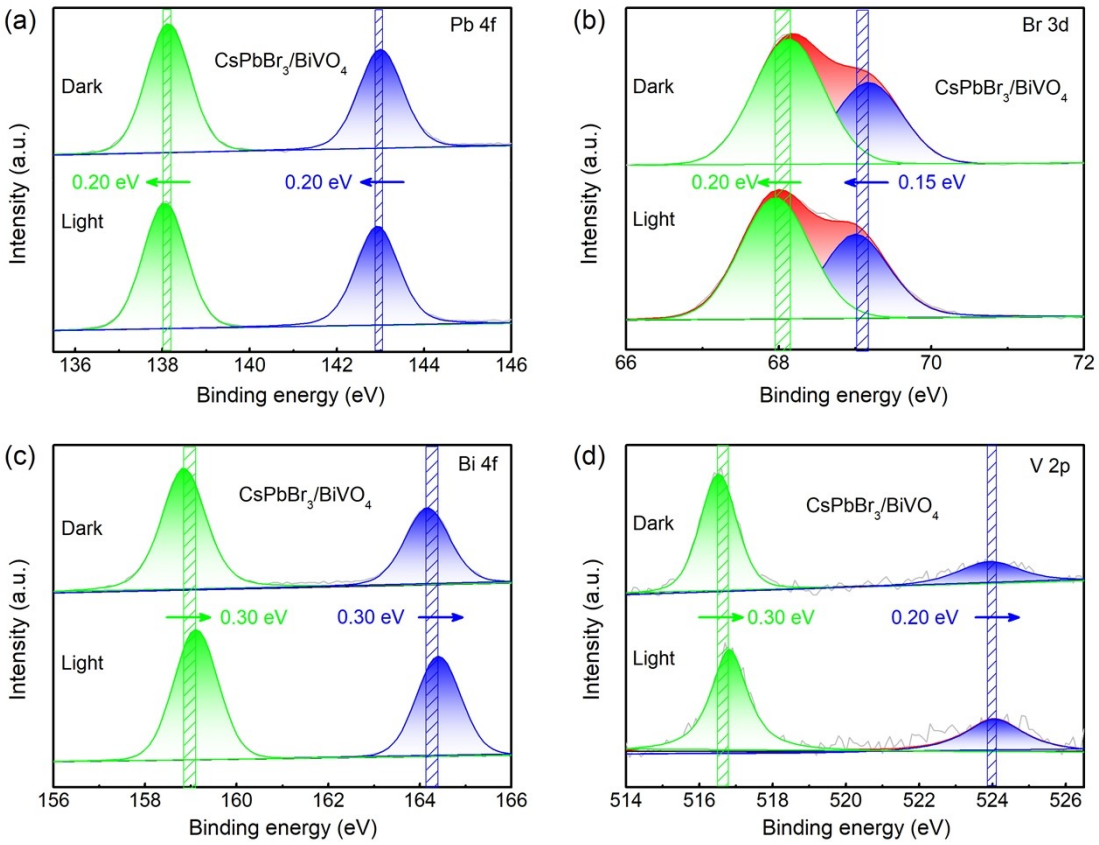

Fig. S10 High-resolution XPS spectra of $CsPbBr_3/BiVO_4$ in the dark and under light irradiation: (a) Pb 4f, (b) Br 3d, (c) Bi 4f, and (d) V 2p.

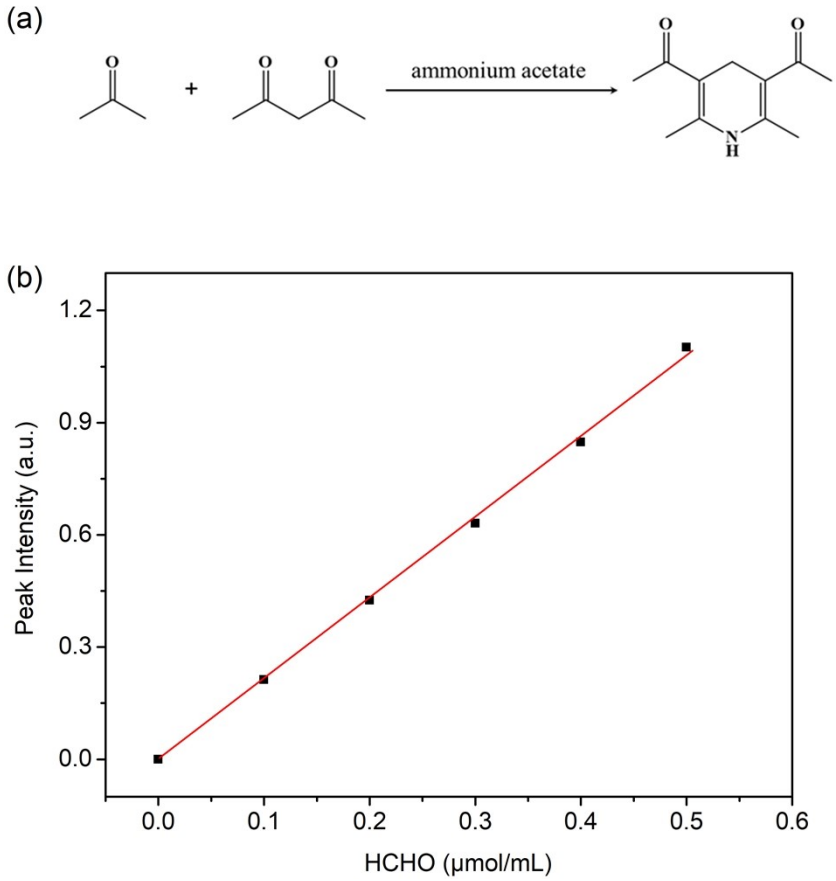

Fig. S11 (a) Reaction mechanism on acetylacetone color developing method to detect HCHO. (b) Calibration curve for the quantification of HCHO by colorimetric method.

The quantitative determination of HCHO in aqueous solution through the acetylacetone method[S1] is based on the Hantzsch reaction principle. In the presence of excessive ammonium salt, HCHO will react with acetylacetone and ammonia to form yellow-colored 3,5-diacetyl-1,4-dihydrolutidine, which possesses characteristic absorption peak at 413 nm, and the absorption peak intensity is proportional to the concentration of HCHO.

Table S1 Multiexponential fitting parameters for the time-resolved PL decay traces (Fig. 3b). Excitation wavelength: 400 nm; detection wavelength: 520 nm[a].

Sample	τ_1 (ns) (A_1)	τ_2 (ns) (A_2)	τ_3 (ns) (A_3)	τ_{Ave} (ns)
$CsPbBr_3$	3.02 (14.68%)	11.54 (41.60%)	73.19 (43.72%)	37.2
$CsPbBr_3/BiVO_4$	1.22 (16.57%)	5.82 (36.63%)	25.37 (46.80%)	14.2
$Mn@CsPbBr_3/BiVO_4$	1.06 (11.67%)	3.91 (37.33%)	19.27 (51.00%)	11.4
$BiVO_4$	0.48 (81.68%)	3.70 (12.81%)	43.22 (5.51%)	3.2

[a] $A_1+A_2+A_3=1$; The calculation formula of average lifetime $\tau_{Ave} = \sum \tau_i * A_i$

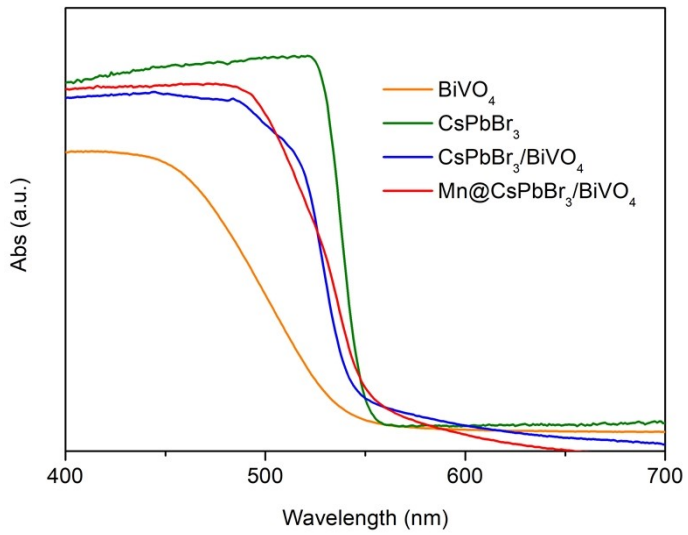

Fig. S12 UV−Vis DRS spectra of $BiVO_4$, $CsPbBr_3$, $CsPbBr_3/BiVO_4$ and $Mn@CsPbBr_3/BiVO_4$.

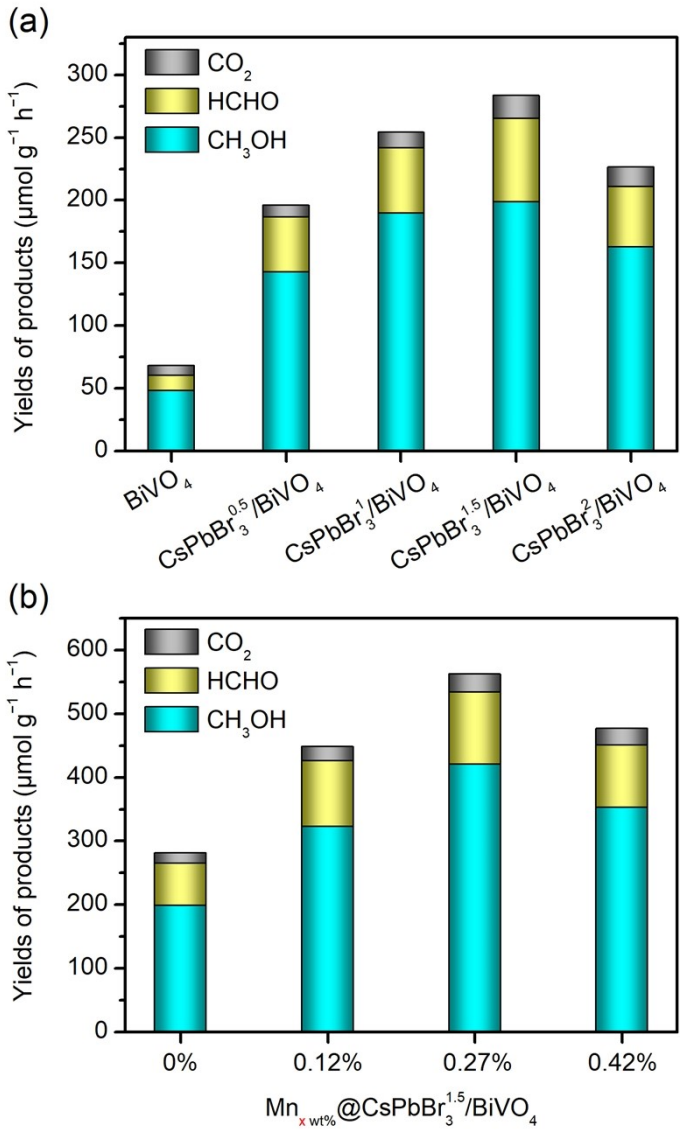

Fig. S13 (a) Yields of oxygenated products with $BiVO_4$ and $CsPbBr_3^x/BiVO_4$ as photocatalysts. (b) Yields of oxygenated products with $Mn_{x\%}@CsPbBr_3^{1.5}/BiVO_4$ composites as photocatalysts.

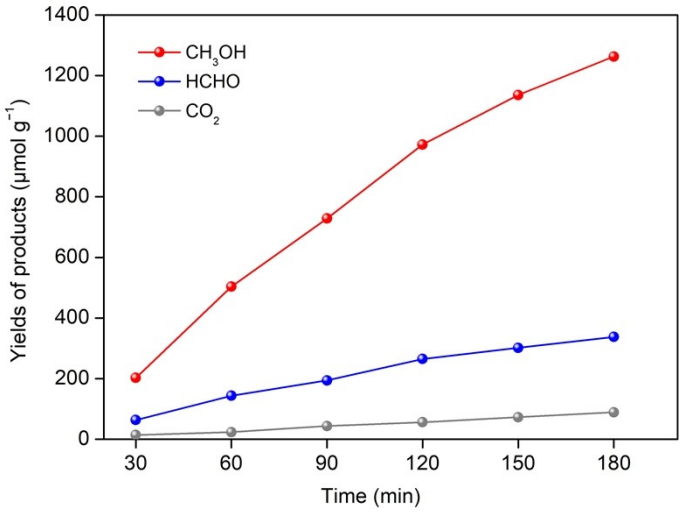

Fig. S14 Variation of photocatalytic products yields over time with Mn@$CsPbBr_3$/$BiVO_4$ as photocatalyst.

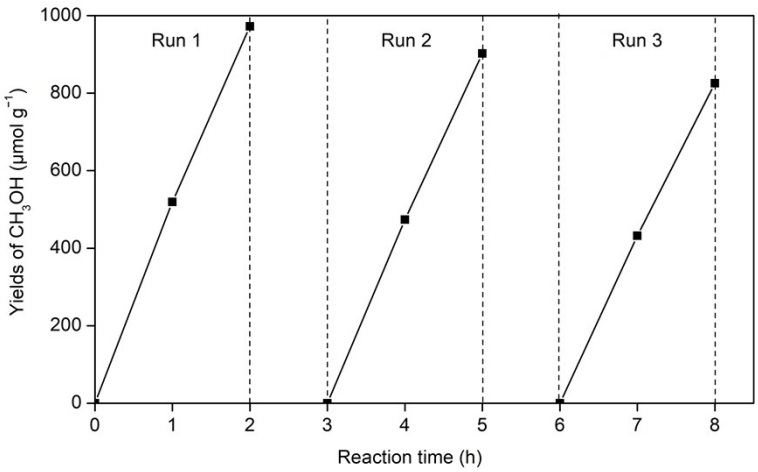

Fig. S15 The results of three runs of CH_4 conversion by Mn@$CsPbBr_3$/$BiVO_4$.

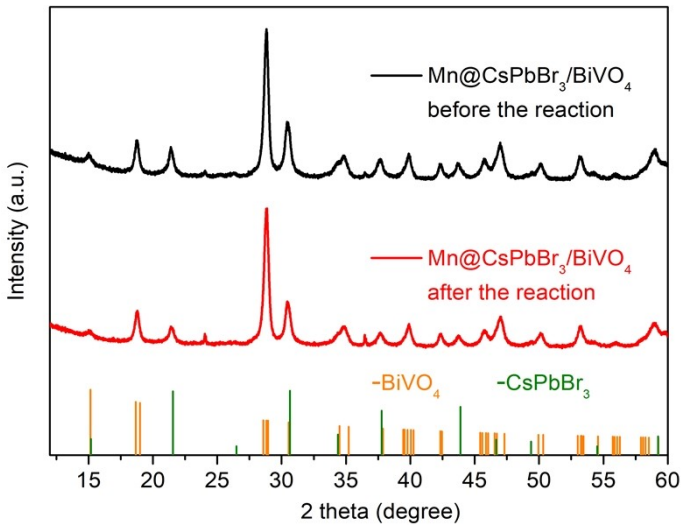

Fig. S16 XRD patterns of $Mn@CsPbBr_3/BiVO_4$ before (black) and after (red) the photocatalytic reaction.

Table S2 Performance comparison with other catalysts for CH_4 photooxidation under similar mild conditions.

Co-catalyst/ photocatalyst	P (atm) /T (℃)	Reactants	Illumination conditions	Main Products (μmol g^{-1} h^{-1}) and selectivity	Ref.
Mn@$CsPbBr_3$/$BiVO_4$	1/25	CH_4, air, H_2O	300 W Xe lamp $\lambda \geq 400$ nm, light intensity 100 mW m^{-2}	CH_3OH: 452.4 HCHO: 112.6 (94.8%)	This Work
ZnO/Fe_2O_3	1/25	CH_4, H_2O	300 W Xe lamp light intensity 100 mW m^{-2}	CH_3OH: 118.84 (99.6%)	S2
Bi_2WO_6 flowers	1/55	CH_4, H_2O	450W Hg lamp	CH_3OH: 15.0 (29.3%)	S3
Bi_2WO_6/TiO_2 composite	1/55	CH_4, H_2O	450W Hg lamp	CH_3OH: 10.8 (7.9%)	
$BiVO_4$ thick platelets	1/55	CH_4, H_2O	450W Hg lamp	CH_3OH: 21.0 (51%)	
Cu-0.5/PCN	1/25	CH_4, H_2O	500 W Xe lamp	CH_3OH: 5.5 C_2H_5OH: 21.0 (52.9%)	S4
FeO_x/TiO_2	1/25	CH_4, H_2O, H_2O_2	300 W Xe lamp	CH_3OH: 352 (79%)	S5
La-WO_3	1/55	CH_4, H_2O	Medium-pressure Hg lamp	CH_3OH: 36.7 (46%)	S6
$BiVO_4$/V_2O_5	1/70	CH_4, H_2O	450 W Hg lamp	CH_3OH: 10.7 (6.4%)	S7
WO_3 mesoporous	1/55	CH_4, H_2O	450 W Hg lamp	CH_3OH: 55.5 (37.4%)	S8
$BiVO_4$ bipyramids	1/65	CH_4, H_2O	350 W Xe lamp	CH_3OH: 111.9 (85%)	S9
FeOOH/m-WO_3	1/25	CH_4, H_2O_2	300 W Xe lamp $420 \leq \lambda \leq 780$ nm	CH_3OH: 211.2 (91%)	S10
C_3N_4-$Cs_{0.33}WO_3$	1/25	CH_4, O_2, H_2O	350 W Xe lamp	CH_3OH: 4.375 (38.1%)	S11

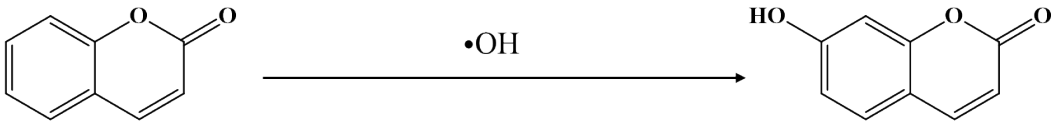

Fig. S17 Reaction mechanism of the •OH detection by coumarin[S12].

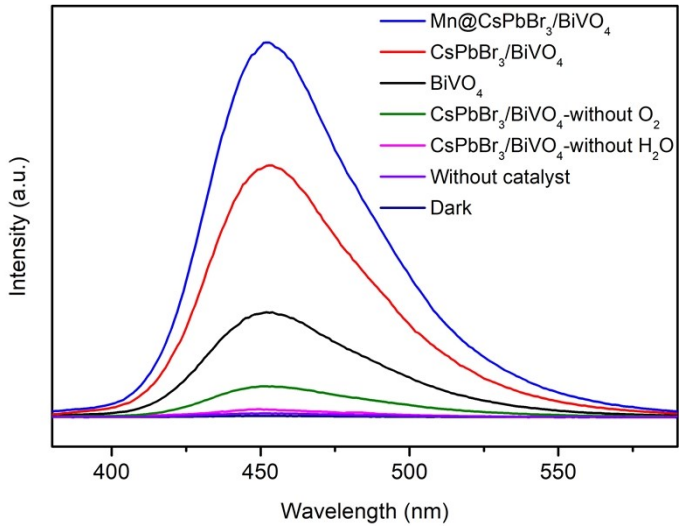

Fig. S18 Fluorescence spectra of coumarin solution with different photocatalysts and reaction conditions.

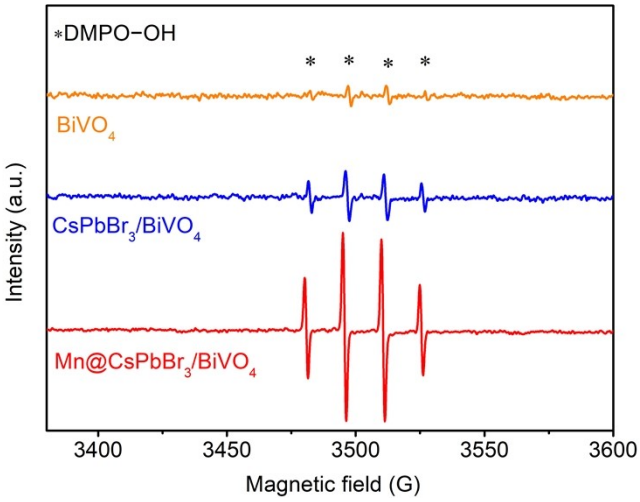

Fig. S19 EPR spectra of DMPO−OH with different photocatalysts under light irradiation for 5 min in the mixture of acetonitrile and water. DMPO was added into the reaction mixture as the radical trapping agent.

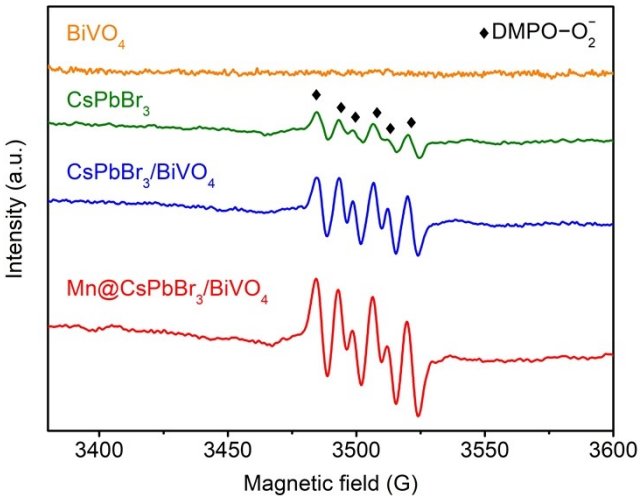

Fig. S20 EPR spectra of DMPO−O_2^- with different photocatalysts under light irradiation for 5 min under O_2 dissolved in reaction solution. DMPO was added into the reaction mixture as the radical trapping agent.

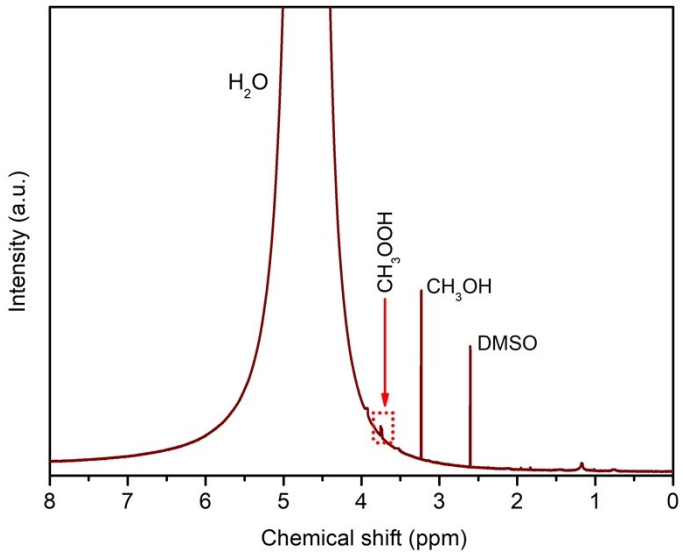

Fig. S21 ^{1}H NMR spectrum (DMSO was added as an internal standard) of the liquid products obtained from photocatalytic methane oxidation over $Mn_{0.27\%}$@$CsPbBr_3/BiVO_4$. Reaction conditions: 30 mg photocatalyst, 500 μL H_2O, mixture of CH_4 and air (gas ratio CH_4/air: 10/1), 8 h irradiation of Xe-lamp with a 400 nm filter at room temperature and a light intensity of 100 mW cm^{-2}.

Table S3 Results of photocatalytic H_2O_2 production.

Entry	Catalyst	Reactant	H_2O_2 (μmol)[a]
1	$BiVO_4$	Air, H_2O	6.52
2	$CsPbBr_3$	Air, H_2O	0
3	$CsPbBr_3/BiVO_4$	Air, H_2O	0
4	$Mn@CsPbBr_3/BiVO_4$	Air, H_2O	0

Reaction conditions: 50 mg photocatalyst, 10 mL acetonitrile, 500 μL H_2O, 15 h irradiation of Xe-lamp with a 400 nm filter at room temperature and a light intensity of 100 mW cm^{-2}

a. Determined by liquid chromatography with reference to the following reaction mechanism：

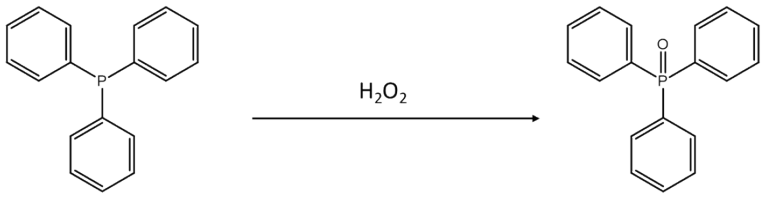

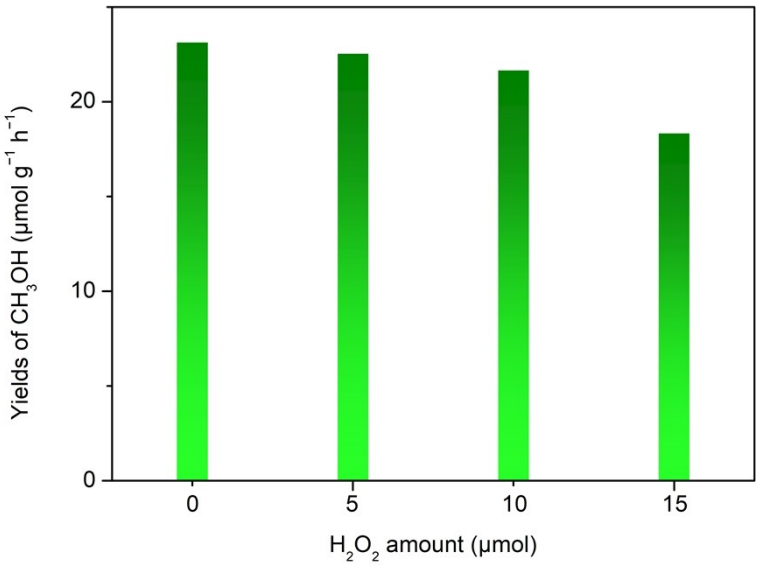

Fig. S22 Yields of CH_3OH by varying H_2O_2 amount with $BiVO_4$ as photocatalyst. Reaction conditions: 10 mg $BiVO_4$, 500 μL H_2O, mixture of CH_4 and air (gas ratio CH_4/air: 10/1), 3 h irradiation of Xe-lamp with a 400 nm filter at room temperature and a light intensity of 100 mW cm^{-2}.

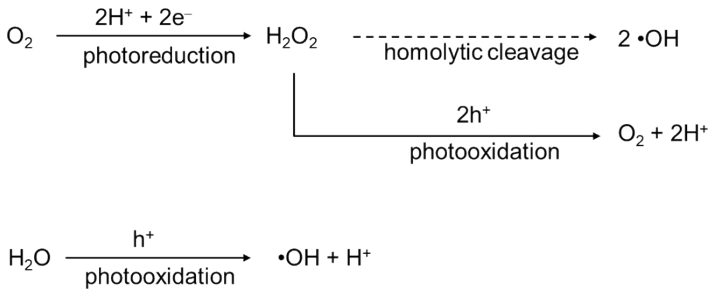

Fig. S23 The processes of electron, hole and proton transfer in the formation of •OH radical with O_2 and H_2O.

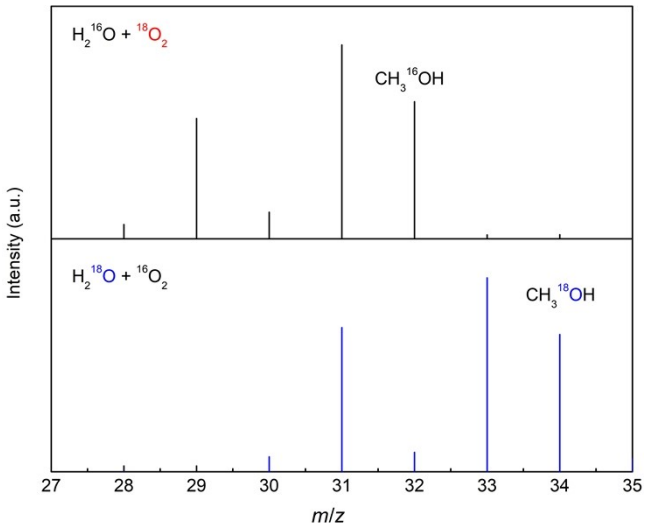

Fig. S24 Mass spectra of CH_3OH generated over $BiVO_4$ with $^{18}O_2 + H_2{}^{16}O$ (top) or $^{16}O_2 + H_2{}^{18}O$ (below) as feedstocks.

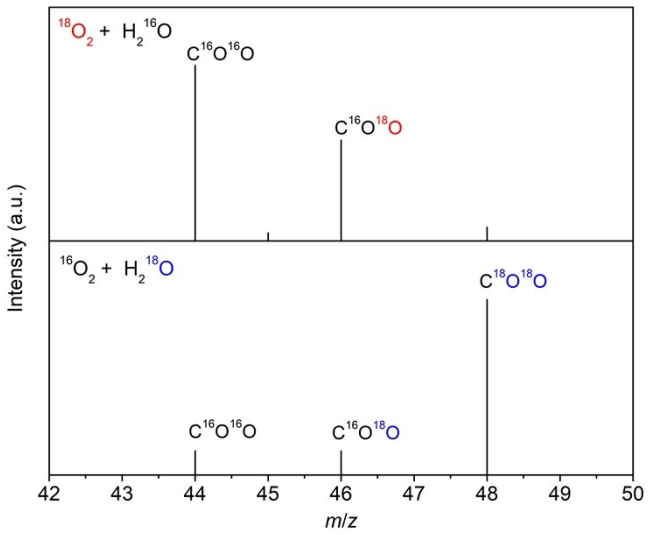

Fig. S25 Mass spectra of CO_2 generated over $Mn_{0.27\%}$@$CsPbBr_3$/$BiVO_4$ with $^{18}O_2$ + $H_2{}^{16}O$ (top) or $^{16}O_2$ + $H_2{}^{18}O$ (below) as feedstocks.

References

S1 J. Chen, S. Stepanovic, A. Draksharapu, M. Gruden and W. R. Browne, *Angew*. *Chem*. *Int*. *Ed*., 2018, **57**, 3207−3211.

S2 K. Zheng, Y. Wu, J. Zhu, L. Li, S. Wang, M. Fan, J. Hu, W. Yan, J. Zhu, Y. Sun and Y. Xie, *J*. *Am*. *Chem*. *Soc*., 2022, **144**, 12357−12366.

S3 S. Murcia-Lopez, K. Villa, T. Andreu and J. R. Morante, *ACS Catal*., 2014, **4**, 3013−3019.

S4 Y. Zhou, L. Zhang and W. Wang, *Nat*. *Commun*. 2019, **10**, 506.

S5 J. Xie, R. Jin, A. Li, Y. Bi, Q. Ruan, Y. Deng, Y. Zhang, S. Yao, G. Sankar and D. Ma, *Nat*. *Catal*., 2018, **1**, 889−896.

S6 K. Villa, S. Murcia-López, J. R. Morante and T. Andreu, *Appl*. *Catal*. *B*, 2016, **187**, 30−36.

S7 S. Murcia-López, M. C. Bacariza, K. Villa, J. M. Lopes, C. Henriques, J. R. Morante and T. Andreu, *ACS Catal*., 2017, **7**, 2878−2885.

S8 K. Villa, S. Murcia-López, T. Andreu and J. R. Morante, *Appl*. *Catal*. *B*, 2015, **163**, 150−155.

S9 W. Zhu, M. Shen, G. Fan, A. Yang, J. R. Meyer, Y. Ou, B. Yin, J. Fortner, M. Foston, Z. Li, Z. Zou and B. Sadtler, *ACS Appl*. *Nano Mater*., 2018, **1**, 6683−6691.

S10 J. Yang, J. Hao, J. Wei, J. Dai and Y. Li, *Fuel*, 2020, **266**, 117104.

S11 Y. Li, J. Li, G. Zhang, K. Wang and X. Wu, *ACS Sustain*. *Chem*. *Eng*., 2019, **7**, 4382−4389.

S12 Q. Xiang, J. Yu and P. K. Wong, *J*. *Colloid Interface Sci*., 2011, **357**, 163−167.